Waste to health: Ag-LTA zeolites obtained by green synthesis from diatom and rice-based residues with antitumoral activity

Wesley F. Monteiro [a], Fernando M. Diz [b], Lucille Andrieu [a], Fernanda B. Morrone [c], Rosane A. Ligabue [b], Katia Bernardo-Gusmão [a], Michèle O. de Souza [a], Anderson J. Schwanke [a],*

[a] *Universidade Federal do Rio Grande do Sul – UFRGS, Instituto de Química, Porto Alegre, Rio Grande do Sul, 91501-970, Brazil*
[b] *Programa de Pós-Graduação em Engenharia e Tecnologia de Materiais, Pontifícia Universidade Católica do Rio Grande do Sul, PUCRS, Porto Alegre, Rio Grande do Sul, 90619-900, Brazil*
[c] *Escola de Ciências da Saúde e da Vida, Pontifícia Universidade Católica do Rio Grande do Sul, PUCRS, Porto Alegre, Rio Grande do Sul, 90619-900, Brazil*

ARTICLE INFO

ABSTRACT

An eco-friendly approach to obtain LTA-type zeolites has been developed using biosilica-based sources derived from industrial wastes, rice husks and diatoms. Both are residues derived from the milling industry with no commercial value. The type of silica was determined in the synthesis of LTA-type zeolites with relative crystallinities of 98 and 48% and cubic crystal sizes of 1.2 and 2.5 µm, respectively. The LTA zeolites and their silver-exchanged derivatives were evaluated for the first time to treat the human bladder cancer cell line T24. The Ag-LTA synthesized with rice husks, diatoms, or commercial silica materials have a vital role of the cytotoxicity of the T24 human bladder cells with reduction of cell viability of 77, 69 and 50%, respectively. The significance of this work lies in the fact that industrial wastes can be transformed into potential zeolitic materials applied in fields not usually explored, such as biomedical, for new anticancer therapies.

1. Introduction

In the field of biomedicine, the production of materials applied for anticancer treatment remains an important area of scientific research. The World Health Organization (WHO) reports that cancer is the second leading cause of death globally, accounting for approximately 9.6 million deaths occurred in 2018 [1]. Bladder cancer is the tenth most common cancer with an estimated 549,000 new cases and 200,000 deaths worldwide (highest rates are observed in Europe and North America), being a type of urological tumor with relatively high morbidity and recurrence metastasis rate [2–4]. In general, the most common therapy after transurethral resection of bladder tumor (TURBT) is immunotherapy using Bacillus Calmette-Guerin (BCG). However, BCG is ineffective in 30% and 40% of patients with nonmuscle invasive bladder cancer (NMIBC), and its use is limited due to the side effects, tumor recurrence, and progression during therapy [5,6]. About 70% of bladder cancer cases are NMIBC (stage Tis, Ta and T1), that in general are not lethal while 30% are muscle-invasive (stage T2, T3, and T4) which can rapidly progress to become metastatic and lead to death [7]. T24 cells are a cell line derived from a patient with high-grade and invasive human urinary bladder cancer and belongs to one category of urinary bladder epithelial transitional carcinoma cells. This type of tumor is difficult to treat and patients have less than five-year survival rates [8].

The use of silver nanomaterials has become one of the most predominant biomedical applications in the emerging field of nanotechnology to eliminate cancer cells [9,10]. The materials' biological activity depends on factors such as surface chemistry, size, shape, distribution, and morphology particles, among others [11]. Recent studies have focused on the development of silver nanoparticles (AgNPs) evaluating their effect on the different cancer cells. The results accessed by MTS assay in MNHK45 gastric cancer cells indicated reductions of more than 60% in cell viability, while in the case of MCF-7 breast cancer cells, the reduction in viability was above 70% [12,13]. Comparing AgNPs of different sizes (20, 80, and 130 nm) and ionic silver revealed that AgNPs with 20 nm were the most efficient, reducing the integrity of L929 fibroblast cells membranes. In contrast, ionic silver was more efficient than all AgNPs, reducing the cell membrane integrity of RAW 264.7 macrophages [14]. In erythroid cells, AgNPs affects histone modifications and gene expression reducing the β-globin transcription through

---

* Corresponding author.
  E-mail address: anderson-js@live.com (A.J. Schwanke).

diminishing methylation of H3K4me3 and H3K79me1, while ionic Ag did not show changes in histone modifications [15].

For antimicrobial activity, the primary mechanism is based on the release of Ag^+ ions from the AgNPs and its interaction with sulfur-containing proteins in the bacterial cell wall, which compromises its functionality [16–18]. For cancer cells, one possible mechanism is based on the generation of reactive oxygen species (ROS) provided by AgNPs, which acted as a source of Ag^+ ions inside the cell and induces oxidative stress leading to damage of cellular components (membrane, protein or DNA) [19]. In this context, the direct use of Ag^+ ions for cancer treatment might be desirable but requires an adjuvant that allows the introduction of silver in its ionic form into the organism.

Zeolites are a class of inorganic molecular sieves applied as ion-exchangers, adsorbents, and catalysts. These materials are built from SiO_4 and AlO_4^- units linked to each other by oxygen bridges which form channels and cavities with molecular dimensions where charge compensating cations neutralize the residual negative charge of the zeolitic structure. The zeolite A (LTA code) is one of the most important industrial zeolites, offering high cation exchange capacity (because of its low Si/Al ratio ~1), and is synthesised easily without using costly organic structure directing-agents [20]. Therefore, LTA zeolite is an excellent candidate to act as an adjuvant to obtain silver in ionic form.

Zeolites obtained by green synthesis is one aspect of green chemistry which has been receiving increased attention and aims to replace commercial reagents with alternative, low-cost, or waste sources [21]. For sources of commercial silica, most of the reactants are not considered environmentally friendly because they require several purification treatments associated with the use of reactants, labor, and residue production [17]. Rice husk is an example of an abundant agro-waste and amorphous silica that could be obtained after a thermal treatment to remove its lignocellulosic compounds [22]. The use of silica from rice husks is promising for rice producing countries. For example, Brazil is one of the biggest rice producers worldwide (the first in the American continent), producing approx. 10.5 million tons in 2019. Rio Grande do Sul, the southernmost state of Brazil, is responsible for producing 70% [23,24]. Since approximately 35% of this quantity corresponds to the ash originated from power plants where the husk is burned, in 2019 approx. 2.6 million tons of silica-based waste has been produced in this state alone. The economic viability for using silica from rice husk is now established, as its production from rice husk ash is now performed industrially. Recently, the new Oryzasil plant, located at Itaqui (Rio Grande do Sul - Brazil) has a production capacity of 28 thousand tons of silica per year [25].

Another example of a source of natural silica is the diatoms, which are microscopic prehistoric porous skeletons of fossilized carapace algae formed by the deposits of silica shell on their structures. The diatoms find their major use as filtering devices, filler, or abrasive agent [26]. After calcination for the removal of organic content, the raw material is classified according to their size and color at the diatom milling industry. However, those with incorrect particle sizes or colors are discarded leading to an important accumulation of waste that contains essentially only silica.

Zeolites synthesized from silica source originated from rice husks, or diatoms have been previously reported. However, those studies are usually focused on the synthesis parameters [27–36] and more recently, applications in catalysis [37–40] and adsorption [41–43]. The literature is scarce on the utilization of zeolites for anti-cancer application and only includes the use of commercially available zeolite A (LTA) [44], X, and Y (FAU) [45,46]. Only one study reports the use of ZSM-5 (MFI) produced from silica of rice husks [47] that focused on *in vitro* application on human colon and epithelial lung cell lines. Therefore, new applications for green zeolites in the field of anti-cancer agents are appealing.

This study intends to demonstrate that the application of zeolites produced through sustainable sources could reach applications other than in the fields of catalysis and adsorption as they are well-established pillars of industry (traditional uses: petrochemistry, chemicals synthesis, purification, among others). Investigating new applications in the field of biomedicine for zeolites produced from industrial waste could be surprising as the waste conversion is usually associated with large-scale processes and not with more noble applications such as medical treatments. Testing zeolite-based materials, produced from silica contained in industrial wastes as antitumor material, is innovative and shows how value can be added to compounds that currently cause environmental issues. This work describes for the first time the use of silver-loaded LTA zeolites synthesized from silica contained in diatom and rice-husk wastes as antitumor material for human T24 bladder cancer cells. The tests were performed *in vitro* and compared with the action of $AgNO_3$ and cisplatin (chemotherapy used for the treatment of bladder cancer). Thus, the aim of this study is to know if the simplest zeolites structures (LTA), synthesized with silica from wastes, can act as carrier and delivery systems of ionic silver for antitumor activity of human bladder cancer cells.

2. Experimental

2.1. Preparation of zeolites

2.1.1. The biosilica sources

The rice husks were provided by rice farmers located in Itaqui, RS, Brazil. The raw material was thermally treated at 600 °C for 5 h (heating rate of 3 °C min⁻¹) under atmospheric air flow, and the product was named "R". The diatom was provided by a diatom milling industry located in Rio do Fogo, RN, Brazil. This material is considered a waste and was discarded after thermal treatment at 850 °C since it presents inadequate requirements (as particle size and color) to be marketed. Here, the diatom was named "D". Commercial silica fumed (Sigma-Aldrich) was used as a reference for the traditional synthesis and named "C".

2.2. Synthesis of LTA zeolites

The synthesis of LTA zeolites was performed according to the literature [30]. In short, 32.0 mL of a 0.234 mol L⁻¹ solution of sodium hydroxide (NaOH, Nuclear) was divided into two beakers, A and B. In the beaker A, 3.30 g of sodium aluminate (NaAlO₂, Sigma-Aldrich) was added and kept under stirring until complete dissolution. In beaker B, 1.78 g of silica (R, D, or C) and 2.34 g of NaOH were added and stirred for 15 min. The solution of beaker A was transferred into beaker B and stirred for 15 min. Then the gel was added into a sealed Teflon vessel and kept in the oven for 4 h at 100 °C. Afterward, the sealed Teflon vessel was quenched in cold water, and the material was filtered until pH 7 and dried at 80 °C for 18 h. All of the following procedures were performed in darkness to avoid reducing ionic silver Ag^+ to metallic silver Ag^0. To obtain silver-ion exchanged LTA zeolites, a solution of $AgNO_3$ (Vetec, 99.9%, 100 mL, 1.5% of Ag) was added with 1 g of zeolite at room temperature for 16 h with stirring. Afterward, the solids were filtered, dried at 100 °C, and stored in darkness flasks.

The calcium ion-exchange experiments were performed according standard procedure [48] with the pristine LTA-R, LTA-D, and LTA-C zeolites mixing 0.5 g of zeolite and 5 mL of a CaCl₂ solution (0.1 mol L⁻¹) at 80 °C for 16 h. The solids were filtered with a 0.45 μm Milipore filter and washed successively until the solution does not indicate the presence of Cl⁻ ions, using the $AgNO_3$ test. The materials were labeled as Ca-LTA-X, where X = R, D, or C.

2.3. Preparation of the in vitro assays

2.3.1. Reagents

RPMI-1640, fetal bovine serum (FBS), Fungizone®, penicillin/streptomycin and 0.5% trypsin/EDTA solution were sourced from Gibco Laboratories (Carlsbad, USA). Silver nitrate, $AgNO_3$ (Vetec, 99.9%) and

Fauldcipla, Libbs, 1 mg mL^{-1} of Cisplatin.

2.3.2. Cell culture conditions

The human bladder cancer cells line T24 were obtained from ATCC (Rockville, MD, USA) and maintained in culture medium RPMI-1640 supplemented with 10% (v/v) fetal bovine serum, 1% (v/v) antibiotic (penicillin/streptomycin) and 0.1% (v/v) fungizone. Cells were cultured in a 5% CO_2, 95% air atmosphere at 37 °C.

2.3.3. Preparation of zeolites for treatment

All the zeolites used in this study were suspended in culture medium RPMI-1640 at a concentration of 1000 μg mL^{-1} and serially diluted in different concentrations (25, 50, 100, and 200 μg mL^{-1}). To ensure the suspension uniformity, they were stirred on vortex agitation before every use.

2.3.4. In vitro cell viability by MTS

Cell viability was determined by the MTS (3-(4,5-dimethylthiazol-2-yl)-5 (3-carboxymethonyphenol)- 2-(4-sulfophenyl)-2H-tetrazolium) assay to determine the number of viable cells. Since reduction of MTS salt can only occur in metabolically active cells the level of activity is a measure of the mitochondria's viability. Thus, any increase or decrease in the viable number of cells can be detected by measuring the formazan concentration reflected in the optical density (absorbance at 490 nm) [49]. For evaluation of cell viability, the T24 lineage was plated at a density of 5×10^3 cells per well in 96-well plates. After confluence, T24 cells were treated with different concentrations of the zeolites (25, 50, 100, and 200 μg/mL) and incubated for 24 h. After this period, 20 μL per well of the MTS solution was added. After 2 h of incubation, the optical density of staining was determined by spectrophotometry at 490 nm. The results were determined as a percentage of the absorbance of the treated in relation to the group that did not receive treatment (control).

2.3.5. Statistical analyses

The statistical test used was a one-way analysis of variance (ANOVA), followed by the Tukey post hoc test. Results were presented as the standard error of the mean. GraphPad Prism 5.0® program was used to generate graphs. P values < 0.05 were taken to indicate statistical significance.

2.4. Characterization

The morphology of solids was recorded on a field emission scanning electron microscopy (FESEM), model FEI Inspect F50, in the secondary electron beam. The samples were coated with a thin gold film using an ion-sputter. The transmission electron microscopy (TEM) images were performed on a Tecnai, model G2 T20. The samples were deposited on carbon film-coated copper grids of 300 mesh.

The crystalline phases of the solids were analyzed on a X-ray diffractometer Rigaku, model Ultima IV, with Cu-Kα1 (1.54 Å), step size of 0.02 and the 2θ scanned was from 3 to 40°. The relative crystallinity (%) was calculated according to the standard test provided by the ASTM D5357 report, using the sum of the areas of the six most intense reflections at 2θ = 7.1, 10.1, 12.4, 24, 27.1, and 29.9° of the diffractogram of each sample, and of the diffractogram of the sample synthesized with commercial silica LTA-C using equation (1):

$$Relative \ crystallinity \ (\%) = \frac{S_x}{S_r} \times 100 \tag{1}$$

where, S_x is the sum of the peak areas of the sample's diffractogram and S_r the sum of the peak areas of the LTA-C's diffractogram.

The chemical composition of the R and D raw materials was determined by X-ray Fluorescence (XRF) Spectrometry on a Bruker, model S2 Ranger. The R raw material exhibited weight percentage of 93 (SiO_2), 1.9 (Al_2O_3), 1.9 (K_2O), 1.7 (MgO), 1.1 (CaO), 0.2 (Fe_2O_3), and 0.2

(MnO). The D raw material was 92 (SiO_2), 5.5 (Al_2O_3), 1.1 (MgO), 0.7 (Fe_2O_3), 0.5 (Na_2O), and 0.2 (K_2O). The concentration of elements (Si, Al and Fe) was determined by atomic absorption spectroscopy (AAS) on a Perkin Elmer, model AAnalyst 200. The samples were digested in concentrated fluoridric and nitric acid before being measured.

Porosity texture was characterized by N_2 adsorption/desorption isotherms on a Micromeritics, model Tristar II 3020, using a pretreatment under degassing for 12 h at 300 °C before the analyses. The Brunauer-Emmet-Teller methodology was used to calculate the specific surface area a$_{(BET)}$ [50]. The microporous volume (V_{micro}) was estimated by t-plot methodology and the total pore volume (V_{TP}) was determined from the adsorbed amount of N_2 at a relative pressure of 0.99.

3. Results and discussion

The SEM images of rice husks (R) and diatom (D) silica sources are shown in Fig. 1. The R silica image reveals irregular particles with fibrous structures and sizes between 2 and 10 μm, which is typical of silica derived from rice husks [30]. The D silica image shows some flat and fibrous particles larger than 10 μm. Some particles have submicron pores with diameters of approximately 285 nm, as observed in the lower-left corner of the image.

Fig. 2 presents the results of the XRD analysis of the studied solids corresponding to rice husk silica (Fig. 2a), diatom (Fig. 2b), and commercial zeolite (Fig. 2c). For comparison purposes, Fig. 2a shows the XRD patterns of silica from rice husk (R), the zeolite synthesized with silica from the rice husks (LTA-R), and the zeolite LTA-R after ion-exchange with Ag$^+$ (Ag-LTA-R). The R sample diffractogram presents a background in the range 2θ = 15–30°, which indicates that only amorphous silica was obtained after calcination. The XRD LTA-R sample analysis shows the diffraction peaks typical of the LTA topology with a cubic unit cell according to the IZA database [51]. Moreover, the LTA-R diffractogram shows the relative crystallinity of 98%, which confirms that synthesis was successful. The XRD pattern of the Ag-LTA-R sample shows the same peaks of the LTA topology and indicates that the silver ion-exchange procedure did not produce structural modifications in the zeolite structure. In addition, no peaks characteristic of metallic silver or Ag_2O were observed, that could be due to their presence as cationic species or due to the small silver particle size, which could be below the detection limit of the XRD equipment. Peaks with lower intensities were also observed for all silver exchanged LTA zeolites synthesized in this study, which is associated with the presence of silver loaded in the zeolite that alters the nature and position of charge compensating cations [52].

The XRD patterns of diatom (D), LTA zeolite from diatom (LTA-D), and its ion-exchanged derivative (Ag-LTA-D) are shown in Fig. 2b. The D
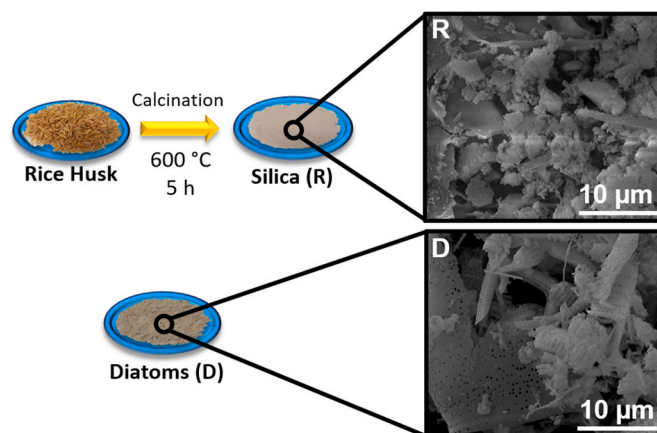

Fig. 1. SEM analysis of raw silica derived from the rice husks (R) and diatom (D).
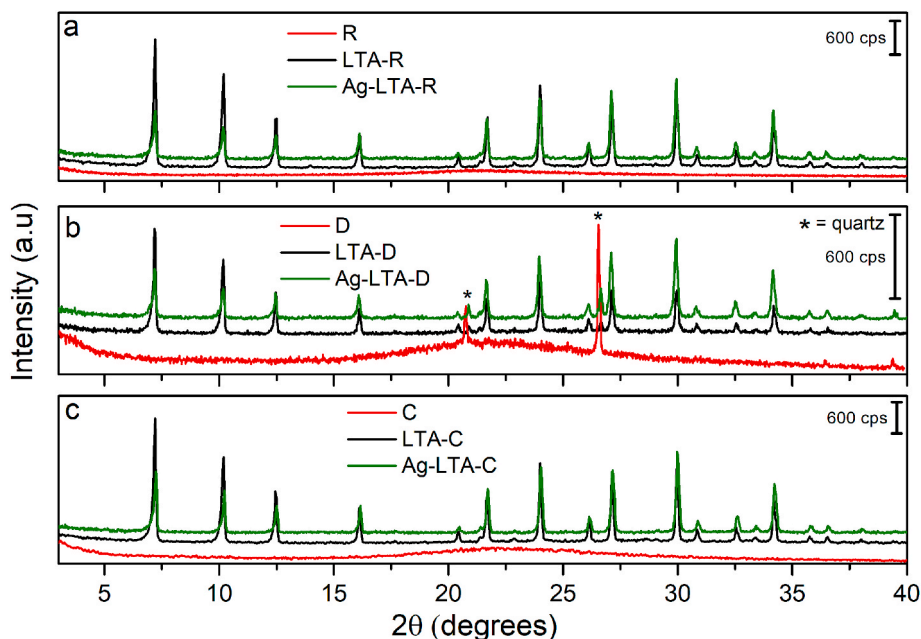
Fig. 2. XRD patterns of R, LTA-R and Ag-LTA-R (a), D, LTA-D, Ag-LTA-D (b) and C, LTA-C, Ag-LTA-C (c) samples.

raw material diffractogram presents a background at $2\theta = 15-30°$ assigned to silica with an amorphous structure. Hence, four peaks at $2\theta = 20.8, 26.7, 36.4,$ and $39.3°$ were observed, which are assigned to the α-quartz phase that was probably formed after its calcination in a beneficing stage in industry. The sample LTA-D analysis shows the same peaks of the LTA structure with a relative crystallinity of 48%. Therefore, the difference between LTA-R and LTA-D, such as the particle sizes and structures, is related to the characteristics of each raw material used as a silica source. The SEM comparison of R and D silica reveals that particles of R-silica are smaller than those of the D-silica, which favor its higher reactivity when compared with the D-silica. Moreover, the XRD pattern of R-silica only indicates the presence of silica with an amorphous structure, which facilitates its dissolution and consumption during the synthesis of the zeolite. On the other hand, the XRD pattern of D-

silica reveals not only the presence of amorphous silica, but also of a stable silica phase (quartz), which is difficult to dissolve during the subsequent zeolite synthesis process. Indeed, the XRD pattern of LTA-D present peaks with low intensities at $2\theta = 20.8$ and $26.7°$, which confirms that the quartz phase is still present after the synthesis.

DR UV Vis analyses were performed to identify the silver state in synthesized LTA zeolites, the corresponding results are shown in Fig. 3a. The absence of signals between ≈390 and 500 nm in all samples indicates that there is no presence of Ag in the nanoparticles, which corroborates with the XRD results. These results indicate that the synthesis leads to the obtention of silver cationic species supported on zeolites. However, the Ag-LTA-D spectrum also presents a shoulder between 270 and 370 nm corresponding to the formation of small Ag_m^{n+} aggregates [53].
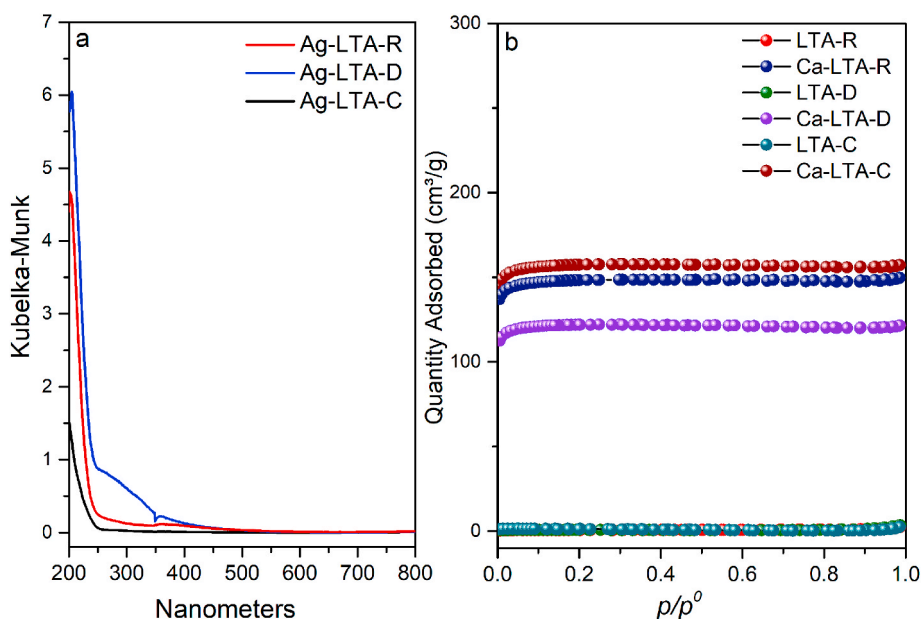

Fig. 3. DR UV Vis of Ag-LTA-R, Ag-LTA-D, Ag-LTA-C (a) and IR N_2 adsorption and desorption isotherms of LTA-R, LTA-D, LTA-C and their derivatives after ion exchange with Ca^{2+} (b).

The N$_2$ adsorption and desorption isotherms of synthesized LTA zeolites are shown in Fig. 3b, and the textural properties determined from these analyses are reported in Table 1 together with the (Si/Al) values determined through AAS analysis. The N$_2$ isotherms reveal that zeolites featured a negligible quantity of N$_2$ adsorbed and are typical of LTA structures containing Na$^+$ as the charge compensating cations, which blocks the pore aperture for the access of N$_2$ molecules [48].

The calcium exchange reaction was performed on LTA zeolites to replace the sodium cations to obtain accurate information about their textural properties. The size of the α-cage of the LTA zeolite increases from 0.31 nm to 0.48 nm due to the replacement of the Na$^+$ per Ca^{2+} cations, enough for rapid uptake of N$_2$ molecules into the LTA zeolite framework micropores. Thus, after the calcium exchange, the adsorbed amount of nitrogen, and consequently, the BET surface increases. Moreover, if this effect is not observed, this gives additional information about the microporous structure, indicating that the zeolite has not been consistently formed.[[30,48,54]]. The comparison of all the textural values of the Na-LTA and Ca-LTA zeolites obtained by N$_2$ adsorption analyses (specific surface area calculated using the BET model, external surface area; microporous volume, and total pore volume) reported in Table 1 confirms this effect.

The corresponding isotherms are of type I, which reveals a microporous nature that is confirmed by the a$_{(BET)}$ values: 605, 498, and 642 m^2 g^{-1} for LTA-R, LTA-D, and LTA-C, respectively. Table 1 shows all samples presented Si/Al molar ratio values between 1 and 2 before and after silver ion-exchange, which is characteristic of the LTA structure [55] and reveals no dealumination after the procedure. Moreover, the iron content of R, D, R-LTA, and D-LTA solids were analyzed because iron could also generate ROS possibly by Fenton-like reactions, causing oxidative stress and apoptosis resulting in cell death [56]. The iron atomic amount in R and R-LTA zeolites are 0.07% and 0.05%, respectively, 0.66 and 0.14% for D and D-LTA samples, respectively. These results have shown that the zeolite produced has the highest purity grade when compared with the silica sources.

The morphology of the synthesized LTA zeolites was evaluated by TEM analysis. In Fig. 4 representative images of each sample. LTA-R image reveals the intergrowth of cubic crystals are presented (crystals with medium sizes of 1.1 μm, and one small crystal of 0.4 μm). Some crystals have irregular surfaces which could indicate that the silica from rice husk was not totally consumed during the synthesis. The SEM image of LTA-D shows a bigger particle with a size of 2.5 μm, which is formed from smaller embedded crystals with sharp edges. The LTA-C image shows the aggregation of three crystals with cubic morphology with medium sizes of 1.5 μm. Unlike the LTA-R and LTA-D samples, these cubic crystals have smoother surfaces and more chamfered edges. The Ag-LTA zeolites were strongly affected by the electron beam in TEM analysis leading to the formation of metallic particles, making the discussion of these results unfeasible.

The results of the SEM analyses of the synthesized Ag-LTA zeolites is

shown in Fig. 5 and reveal that all the samples exhibit crystals with cubic morphology that are typical of LTA structure and according to the TEM images previously described. The LTA-R images also reveal that the large particles have smooth surfaces, but there are some crystals with irregular surfaces, as also previously mentioned in the discussion of the TEM analysis. Furthermore, the intergrowth of cubic crystals with medium sizes of 1.2 μm was observed. The SEM images of Ag-LTA-D zeolite show a larger particle formed by the intergrowth of cubic crystals aggregated randomly. SEM images also reveal that the cubic crystals of LTA-D also possess sharp edged crystals with irregular surfaces where shallow holes can be clearly observed. An intergrowth of some thin and elongated small particles is observed at the lower-left corner of the image, and also in the upper right corner of the inset, which is characteristic of sodalite, a typical concurring zeolitic phase for the LTA zeolite [57]. The SEM image of Ag-LTA-C reveals that cubic crystals with medium sizes of 1.5 μm have smoother surfaces and more chamfered edges than the Ag-LTA-R and Ag-LTA-D zeolites indicating that the type of silica used for the synthesis influences the surface of the crystals formed. Moreover, the intergrowth of small crystals (see inset) was also observed.

Elemental mapping of Ag and Si was performed through SEM-EDS analyses to investigate the distribution of silver in the LTA zeolites. The corresponding images and spectra are reported in Fig. 6. Ag-LTA-R present a homogeneous distribution of silver (green color) into the silica-based material (red color). On the other hand, the mapping image of Ag-LTA-D shows that silver is well distributed, but regions are also observable with higher Ag concentration on some cubic faces which suggests the presence of silver aggregates. These results are in agreement with the results of DR UV Vis (Fig. 3a), which indicated the presence of Ag$_m^{n+}$ aggregates in Ag-LTA-D. We hypothesize that the low crystallinity of the LTA-D zeolite and the surface of some crystals with shallow holes may have favored the aggregation of silver. The atomic percentage of Ag incorporated, estimated by EDS, is 2.2, 2.1, and 3.6% for Ag-LTA-R, Ag-LTA-D, and Ag-LTA-C, respectively.

Bladder cancer is considered one of the worst diseases of the genitourinary tract [58] due to the genomic heterogeneity of bladder cancer which drives the evolution of the tumor and can affect the effectiveness of chemotherapy treatment [59], for example, cisplatin resistance [60]. The human T24 tumor bladder cell line has been used in high cancer malignancy phenotype models since the T24 cells were derived from invasive transitional cell carcinoma with metastatic potential [61]. In recent years, zeolites have been explored in biomedical studies as a new biomaterial due to morphological (*scaffolds*), biochemical, and biocompatible characteristics [62,63]. Moreover, the antitumoral activity of silver was reported for different tumors (*e.g.,* breast cancer, hepatocellular carcinoma, and human skin cancer) [64,65].

In this study, we tested *in vitro* LTA zeolites (with or without silver) obtained by green synthesis from diatom and rice-based wastes as antitumor materials against T24 cells. For comparison purposes, cisplatin which is currently used in chemotherapy [66] and silver ions (AgNO$_3$) which corresponds to un-supported silver cations, were also tested. The cytotoxic study was performed to evaluate the materials over different concentrations (25, 50, 100 and 200 μg mL^{-1}) on the viability of the T24 cells. The corresponding results are shown in Fig. 7 and Table 2.

The data in Fig. 7a shows that cisplatin promoted an inhibitory effect in all concentrations. The high cell death percentage (75.8%) occurred with the use of cisplatin in the highest concentration (200 μg mL^{-1}). This result was expected because, as already mentioned, cisplatin is one of the chemotherapeutic drugs used to treat bladder cancer [66]. On the other hand, silver ions (use of AgNO$_3$) as inhibitory reagent showed only 26.5% of cells death at 200 μg mL^{-1}. This result indicates that cationic silver contained in liquid solutions has a small inhibitory effect, even in high concentrations.

The literature reports the permeability of zeolites with micrometric size through cellular barriers that induce the intracellular oxidative
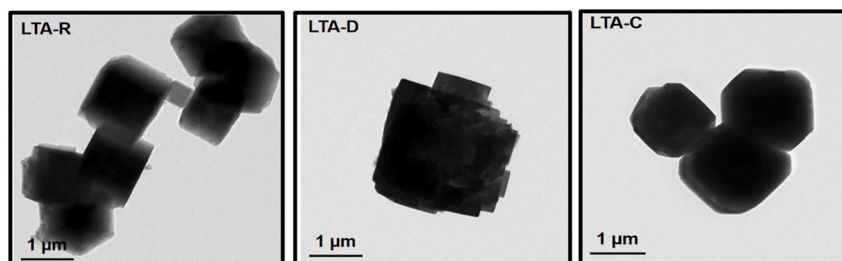
Table 1

Textural properties of synthesized samples obtained from N$_2$ adsorption-desorption analysis and Si/Al ratio (atomic absorption spectroscopy).

Sample	si/al[a]	a$_{(bET)}$[b] (m^2 g^{-1})	a$_{ext}$[c] (m^2 g^{-1})	V$_{micro}$[d] (cm^3 g^{-1})	V$_{TP}$[e] (cm^3 g^{-1})
LTA-R	1.7 (1.2)	3	0.5	0.001	0.005
LTA-D	2.0 (1.3)	4	0	0.001	0.002
LTA-C	1.8 (1.1)	6	0	0.002	0.003
Ca- LTA-R	–	605	30	0.216	0.231
Ca -LTA-D	–	498	24	0.178	0.187
Ca-LTA-C	–	642	31	0.230	0.242

[a] Values in parenthesis correspond to the samples after the silver exchange;
[b] Specific surface area calculated using the BET model;
[c] external surface area;
[d] microporous volume;
[e] total pore volume.

Fig. 4. TEM (a) images of LTA-R, LTA-D and LTA-C zeolites.

Fig. 5. SEM images of Ag-LTA-R, Ag-LTA-D and Ag-LTA-C zeolites.

zeolites. The zeolites act as an ROS generator, and also as a carrier of silver ions leading to a delivery system of silver ions to the cells, which induces the increase in oxidative stress generated by the ROS and results in the growth of cell deaths. The results reported in Fig. 7d show that Ag-LTA-C zeolite' presence promoted an increase in cell viability at a concentration of 50 μg mL^{-1}. This response may be due to normal variations in the physiological mechanisms of cells in baseline conditions, which may be related to cell adaptation exposed to non-toxic zeolite. The objective of these tests being first to highlight the potential of zeolites produced by sustainable sources to treat cancer, a deeper understanding of this result will be the subject of future studies that are crucial to explaining all the effect involved.
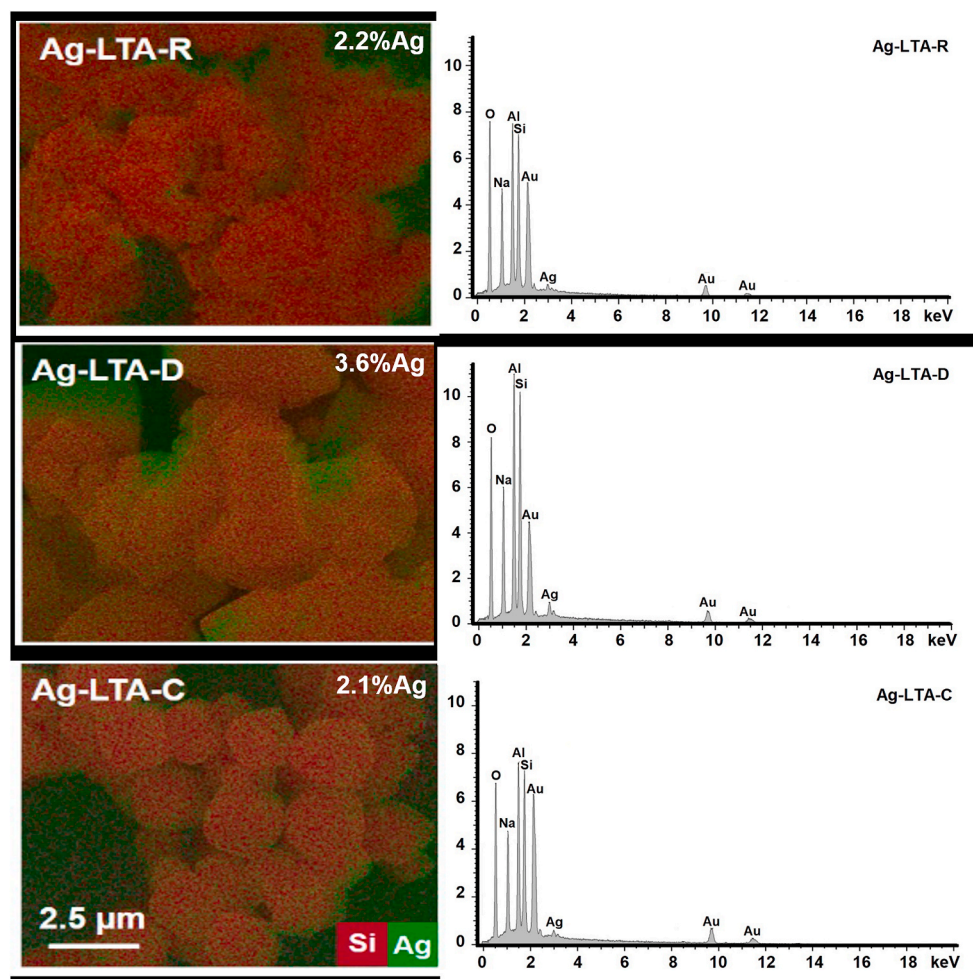
Furthermore, comparing the effect produced by unsupported silver ions (use of AgNO$_3$) with Ag-LTA zeolites added to the cells in the same concentrations, reinforces the evidence of the cooperative influence of the zeolite structure and the silver cations that they contain. Indeed, the concentration of silver ions available in the case of AgNO$_3$ is much higher than in the case of Ag-LTA. An example of this reported in Table 2, is that the best result obtained with AgNO$_3$ added at a concentration of 200 μg mL^{-1} corresponds to cell viability of 73.5% while the presence of any Ag-LTA zeolites in the same concentration leads to cell viability of less than 51%. These results indicate that the unsupported silver ions, even present in higher content, show a smaller inhibitory effect than any Ag-LTA zeolites, and confirm the cooperative influence of the zeolite structure of the Ag-zeolites systems.

The differences in the effects observed between the Ag-LTA samples, *i.e.*, Ag-LTA-R, and Ag-LTA-D zeolites, which present more cell death than Ag-LTA-C (see results in Table 2) could be correlated with the texture of the zeolite crystal surface. One could hypothesize that the presence of sharper edges and irregular surfaces observed by SEM for Ag-LTA-R, and Ag-LTA-D materials (see Fig. 5), may ease the interaction between the Ag-zeolites and the cells. Further studies should be carried out to confirm it.

The comparative UV–vis study of the Ag-zeolites indicated the presence of small silver aggregates in the case of the Ag-LTA-D zeolite. As the cell viability obtained with this zeolite is similar to the result obtained with Ag-LTA-R, when both are added at a concentration of 200 μg mL^{-1}. This result indicates that the Ag-LTA-D zeolite could also act as a carrier and delivery system even if the silver is present as small silver aggregates. Thus, these findings shed light on the possibility of zeolites also acting as delivery and release systems for small silver aggregates and not only for isolated silver cations.

Fig. 7 reveals that, at 200 μg mL^{-1} concentration, the presence of silver in the zeolite is significant and follows the order Ag-LTA-C < Ag-LTA-D < Ag-LTA-R. As observed in EDS results (Fig. 6), the content of silver is higher in Ag-LTA-D than other Ag-zeolites, nevertheless, the activity of Ag-LTA-R is similar or higher than Ag-LTA-D, showing that this activity is more closely related to the synergic effect of Ag in the ionic form with the zeolite than the concentration value of Ag. Hence, the results obtained by Ag-LTA-R and Ag-LTA-D are similar to those found using cisplatin, showing the potentiality of these materials as a possible tool in the future treatment of bladder cancer.

To explore the results of Fig. 7 in more detail, the data of this study

stress by the generation of ROS [67]. Since the bladder cancer cells have sizes of approximately 6 μm [68] and the zeolites synthesized in this study have a micrometric size (LTA-R (1.2 μm), LTA-D (2.5 μm), and LTA-C (1.5 μm)) we performed blank tests with the parent LTA zeolites (LTA-R, LTA-D and, LTA-C) to evaluate the biological affinity of theses zeolites with T24 cells. The results of this study reported in Fig. 7 reveal that no significant cytotoxic effect was registered on the viability of the T24 cells after 24 h at concentrations of 25 and 50 μg mL^{-1}. However, when the highest concentration of LTA is used (200 μg mL^{-1}), a reduction of the viability of approximately 25% for LTA-R and LTA-D, and 30% for LTA-C was observed. These results confirm that LTA zeolites with micrometric crystal size offer affinity with T24 cells.

When Ag-LTA-R, Ag-LTA-D, and Ag-LTA-C zeolites are used in concentrations of 200 μg mL^{-1}, the effect of silver is observed by the decrease in cell viability of 23, 31, and 51%, respectively. Comparing the viability data with those observed when only zeolites are added to the cells, highlights the combined effect between the silver ions and LTA

Fig. 6. SEM-EDS images and spectra of Ag-LTA-R, Ag-LTA-D and Ag-LTA-C zeolites. The elemental mapping indicates the Ag (green color) and Si (red color). (For interpretation of the references to color in this figure legend, the reader is referred to the Web version of this article.)

corresponding to the cell viability (CV) test with 100 and 200 μg mL^{-1} of zeolite (with or without Ag) is reported in Table 2. The difference between the CV obtained with free-Ag-zeolite and Ag-zeolite (□V) was calculated to evaluate the effect of the Ag. The □V values enable us to separate the effect of the LTA zeolites without Ag from the Ag-LTA zeolites on cell viability. Except in the case of the test conducted with 100 μg mL^{-1} of LTA-C, the data in Table 2 demonstrates that Ag increases the antitumoral activity of the zeolites as previously stated. Results of the tests performed with 100 μg mL^{-1} of LTA-C and Ag-LTA-C that show no effect of silver may be associated with the limitations of *in vitro* assays to evaluate cell viability in monolayer (2D) culture.

The highest activity was observed in the silver-modified zeolites Ag-LTA-R and Ag-LTA-D. The best result was achieved with Ag-LTA-R (200 μg mL^{-1}), leading to the death of 76.9% of cells (cell viability equal to 23.1%). This result indicates that silver is responsible for slightly more than half of antitumoral activity of the material. Not least, this result is quite superior to Cisplatin. Moreover, this chemotherapeutic induces toxicity and high rates of resistance [69]. In summary, the antitumoral activity at 200 μg mL^{-1} concentration follows the order: AgNO$_3$ < Ag-LTA-C < Ag-LTA-D < Cisplatin < Ag-LTA-R. This result shows the possibility of synthesizing environmental-friendly materials from industrial waste with biological activity against tumoral cells that could be alternatives compounds for platinum-based drugs.

form) from an environmentally friendly and sustainable method using diatom (LTA-D) and rice-based (LTA-R) wastes as silica sources. Ag-LTA corresponding zeolites were prepared through ion exchange and tested *in vitro* to evaluate their activity for reducing T24 bladder cancer cells. UV–vis characterization of the materials indicated that silver is present in the zeolite as cations (Ag-LTA-R) and small aggregates (Ag-LTA-D). Comparative tests performed on LTA and Ag-LTA zeolites showed that both the zeolite and the silver species reduce T24 bladder cancer cells. The zeolite acts as an ROS generator, and as a carrier of silver ions, becoming a delivery system of silver ions to the cells, which induces the increase in cell deaths. This antitumoral collaborative effect was also evidenced by comparing the biological impact of unsupported silver ions of AgNO$_3$ (26%) added at the concentration of 200 μg mL^{-1} with those of Ag-LTA-R (77%) and, Ag-LTA-D (69%) used in the same weight concentration. The best result was obtained with the Ag-LTA-R zeolite from the concentration of 200 μg mL^{-1} showing antitumoral activity of 77%, near to the result obtained with cisplatin (76%), a current cancer treatment. The antitumoral activity of the studied materials follows the order AgNO$_3$ < Ag-LTA-C (comercial) < Ag-LTA-D ~ cisplatin ~ Ag-LTA-R. The results herein obtained leads one to consider such materials as an environment-friendly alternative to current drugs and to suggest further research into new applications in the pharmaceutical and clinical field.

4. Conclusions

This study shows that it is possible to obtain LTA zeolites (sodium

CRediT authorship contribution statement

Wesley F. Monteiro: Conceptualization, Methodology, Validation,
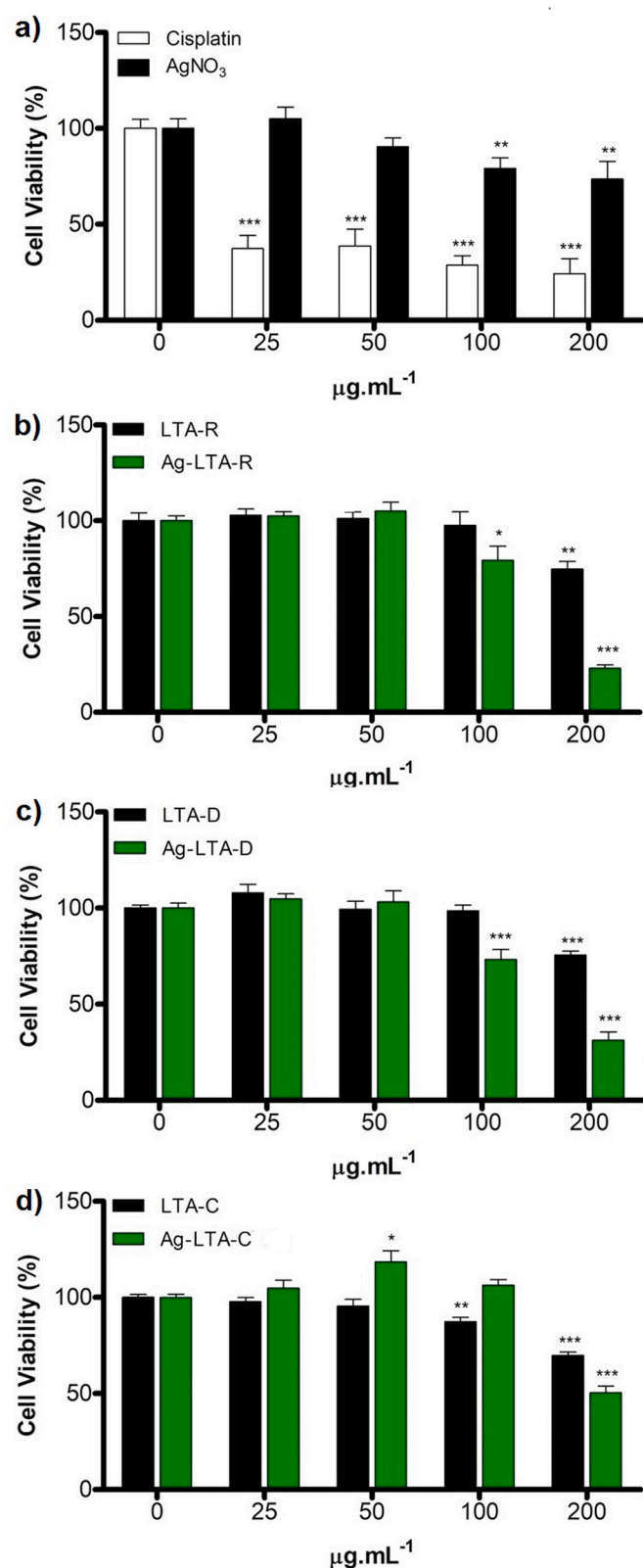
Fig. 7. Evaluation of the antitumor activity of cisplatin and AgNO₃ (a), LTA-R and Ag-LTA-R (b), LTA-D and Ag-LTA-D (c), and LTA-C and Ag-LTA-C (d) materials on the viability of human bladder cancer T24 cells after 24 h. Cell viability was evaluated by MTS assay after treatment with zeolites (0, 25, 50, 100, and 200 $\mu g\ mL^{-1}$). The experiments were performed in triplicate. Each column represents the standard error of mean $\pm$, *$p < 0.05$, **$p < 0.01$, and ***$p < 0.001$, and the results were established in relation to control cells (not treated and considered as 100% of cell viability).

Table 2

Evaluation of the effectiveness of treatment with Cisplatin, AgNO₃, pure and Ag-modified LTA zeolites.

Zeolites	[a]CV (%)	[a]CV (%)	[b]ΔV (%)
	Without Ag	With Ag	
		100 $\mu g\ mL^{-1}$	
LTA-R	100	79.3	20.7
LTA-D	100	73.3	26.7
LTA-C	87.3	100	[c]
		200 $\mu g\ mL^{-1}$	
LTA-R	74.8	23.1	51.7
LTA-D	75.5	31.2	44.3
LTA-C	68.8	50.3	18.5
Reagents		[a]CV (%)	
	100 $\mu g\ mL^{-1}$		
Cisplatin		28.7	
AgNO₃		79.2	
	200 $\mu g\ mL^{-1}$		
Cisplatin		24.2	
AgNO₃		73.5	

[a] Cell viability,

[b] Difference between CV without Ag and CV with Ag,

[c] increase in the cell viability.

Declaration of competing interest

The authors declare that they have no known competing financial interests or personal relationships that could have appeared to influence the work reported in this paper.

Acknowledgements

References

[1] The World Health Organization, Who. https://www.who.int/, 2020 accessed Feb 2020.

[2] H. Qu, B. Ma, H.F. Yuan, Z.Y. Wang, S.J. Guo, J. Zhang, Effect of salinomycin on metastasis and invasion of bladder cancer cell line T24, Asian Pac. J. Trop. Med. 8 (2015) 578–582, https://doi.org/10.1016/j.apjtm.2015.06.004.

[3] F. Bray, J. Ferlay, I. Soerjomataram, R.L. Siegel, L.A. Torre, A. Jemal, Global cancer statistics 2018: GLOBOCAN estimates of incidence and mortality worldwide for 36 cancers in 185 countries, CA, Cancer J. Clin. 68 (2018) 394–424, https://doi.org/10.3322/caac.21492.

[4] J. Afonso, L.L. Santos, A. Longatto-Filho, F. Baltazar, Competitive glucose metabolism as a target to boost bladder cancer immunotherapy, Nat. Rev. Urol. 17 (2020) 77–106, https://doi.org/10.1038/s41585-019-0263-6.

[5] C. Wang, Q. Wang, X. Li, Z. Jin, P. Xu, N. Xu, A. Xu, Y. Xu, S. Zheng, J. Zheng, C. Liu, P. Huang, Lycorine induces apoptosis of bladder cancer T24 cells by inhibiting phospho-Akt and activating the intrinsic apoptotic cascade, Biochem. Biophys. Res. Commun. 483 (2017) 197–202, https://doi.org/10.1016/j.bbrc.2016.12.168.

[6] L. Rockenbach, L. Bavaresco, P. Fernandes Farias, A.R. Cappellari, C.H. Barrios, F. Bueno Morrone, A.M. Oliveira Battastini, Alterations in the extracellular catabolism of nucleotides are involved in the antiproliferative effect of quercetin in human bladder cancer T24 cells, Urol. Oncol. Semin. Orig. Investig. 31 (2013) 1204–1211, https://doi.org/10.1016/j.urolonc.2011.10.009.

[7] J. Zheng, X. Zhu, J. Zhang, CXCL5 knockdown expression inhibits human bladder cancer T24 cells proliferation and migration, Biochem. Biophys. Res. Commun. 446 (2014) 18–24, https://doi.org/10.1016/j.bbrc.2014.01.172.

[8] Y. Zhang, X. Lai, Q. Zeng, L. Li, L. Lin, S. Li, Z. Liu, C. Su, M. Qi, Z. Guo, Classifying low-grade and high-grade bladder cancer using label-free serum surface-enhanced Raman spectroscopy and support vector machine, Laser Phys. 28 (2018) 1–8, https://doi.org/10.1088/1555-6611/aa9d6d.

[9] L. Chen, C. Zhang, J. Xiao, J. You, W. Zhang, Y. Liu, L. Xu, A. Liu, H. Xin, X. Wang, Local extraction and detection of early stage breast cancers through a microneedle and nano-Ag/MBL film based painless and blood-free strategy, Mater. Sci. Eng. C 109 (2020) 110402, https://doi.org/10.1016/j.msec.2019.110402.

[10] N. Pandiyan, B. Murugesan, M. Arumugam, J. Sonamuthu, S. Samayanan, S. Mahalingam, Ionic liquid - a greener templating agent with Justicia adhatoda plant extract assisted green synthesis of morphologically improved Ag-Au/ZnO nanostructure and it's antibacterial and anticancer activities, J. Photochem. Photobiol. B Biol. 198 (2019) 111559, https://doi.org/10.1016/j.jphotobiol.2019.111559.

[11] X.F. Zhang, Z.G. Liu, W. Shen, S. Gurunathan, Silver nanoparticles: synthesis, characterization, properties, applications, and therapeutic approaches, Int. J. Mol. Sci. 17 (2016), https://doi.org/10.3390/ijms17091534.

[12] A.C. Gomathi, S.R. Xavier Rajarathinam, A. Mohammed Sadiq, S. Rajeshkumar, Anticancer activity of silver nanoparticles synthesized using aqueous fruit shell extract of Tamarindus indica on MCF-7 human breast cancer cell line, J. Drug Deliv. Sci. Technol. 55 (2020) 101376, https://doi.org/10.1016/j.jddst.2019.101376.

[13] S.F. Hashemi, N. Tasharrofi, M.M. Saber, Green synthesis of silver nanoparticles using Teucrium polium leaf extract and assessment of their antitumor effects against MNK45 human gastric cancer cell line, J. Mol. Struct. 1208 (2020), https://doi.org/10.1016/j.molstruc.2020.127889.

[14] M.V.D.Z. Park, A.M. Neigh, J.P. Vermeulen, L.J.J. de la Fonteyne, H.W. Verharen, J.J. Briedé, H. van Loveren, W.H. de Jong, The effect of particle size on the cytotoxicity, inflammation, developmental toxicity and genotoxicity of silver nanoparticles, Biomaterials 32 (2011) 9810–9817, https://doi.org/10.1016/j.biomaterials.2011.08.085.

[15] Y. Qian, J. Zhang, Q. Hu, M. Xu, Y. Chen, G. Hu, M. Zhao, S. Liu, Silver nanoparticle-induced hemoglobin decrease involves alteration of histone 3 methylation status, Biomaterials 70 (2015) 12–22, https://doi.org/10.1016/j.biomaterials.2015.08.015.

[16] E. Navarro, F. Piccapietra, B. Wagner, F. Marconi, R. Kaegi, N. Odzak, L. Sigg, R. Behra, Toxicity of silver nanoparticles to Chlamydomonas reinhardtii, Environ. Sci. Technol. 42 (2008) 8959–8964, https://doi.org/10.1021/es801785m.

[17] G.A. Sotiriou, S.E. Pratsinis, Antibacterial activity of nanosilver ions and particles, Environ. Sci. Technol. 44 (2010) 5649–5654, https://doi.org/10.1021/es101072s.

[18] B. Reidy, A. Haase, A. Luch, K.A. Dawson, I. Lynch, Mechanisms of silver nanoparticle release, transformation and toxicity: a critical review of current knowledge and recommendations for future studies and applications, Materials 6 (2013) 2295–2350, https://doi.org/10.3390/ma6062295.

[19] A. Karuppaiah, K. Siram, D. Selvaraj, M. Ramasamy, D. Babu, V. Sankar, Synergistic and enhanced anticancer effect of a facile surface modified non-cytotoxic silver nanoparticle conjugated with gemcitabine in metastatic breast cancer cells, Mater, Today Commun 23 (2020) 100884, https://doi.org/10.1016/j.mtcomm.2019.100884.

[20] Lobo Lobo, in: S.M. Auerbach, K.A. Carrado, P.K. Dutta (Eds.), Introd. To Struct. Chem. Zeolites. Handb. Zeolite Sci. Technol, Marcel Dekker, Inc, New York, Basel, 2003, p. 75, 2003.

[21] E.-P. Ng, X. Zou, S. Mintova, Chapter 12 - Environmental Synthesis Concerns of Zeolites A2 - Suib, Steven L, New and Future Developments in Catalysis, Elsevier, Amsterdam, 2013, pp. 289–310 (2013) 2013.

[22] J. Singh, N. Kaur, P. Kaur, S. Kaur, J. Kaur, P. Kukkar, V. Kumar, D. Kukkar, M. Rawat, Piper betle leaves mediated synthesis of biogenic SnO_2 nanoparticles for photocatalytic degradation of reactive yellow 186 dye under direct sunlight, Environ. Nanotechnology, Monit. Manag. 10 (2018) 331–338, https://doi.org/10.1016/j.enmm.2018.07.001.

[23] https://www.conab.gov.br/info- agro/safras/graos/boletim-da-safra-de-graos (accessed May 2020)CONAB, Companhia Nacional de Abastecimento, Boletim de Safra 2019/20, 2020, 4° levantamento.

[24] FAO Rice Market Monitor (RMM) XXI (Issue No. 1) (2018) XXI.

[25] accessed May 2020, https://www.oryzasil.com.br/pt-br/institucional, 2020.

[26] J.E. Kogel, N.C. Trivedi, J.M. Barker, S.T. Krukowski (Eds.), Industrial Minerals & Rocks: Commodities, Markets, and Uses, seventh ed., Society for Mining, Metallurgy, and Exploration, Littleton, CO, USA, 2006 (2006) 2006.

[27] J.F. Gomes, A. Sachse, J.R. Gregório, K. Bernardo-Gusmão, A.J. Schwanke, Sustainable synthesis of hierarchical MWW zeolites using silica from an agro-

[28] P. Vinaches, A.J. Schwanke, C.W. Lopes, I.M.S. Souza, J. Villarroel-Rocha, K. Sapag, S.B.C. Pergher, Incorporation of Brazilian diatomite in the synthesis of an MFI zeolite, Molecules 24 (2019) 1–13, https://doi.org/10.3390/molecules24101980.

[29] G. Garcia, E. Cardenas, S. Cabrera, J. Hedlund, J. Mouzon, Synthesis of zeolite y from diatomite as silica source, Microporous Mesoporous Mater. 219 (2016) 29–37, https://doi.org/10.1016/j.micromeso.2015.07.015.

[30] D.I. Petkowicz, R.T. Rigo, C. Radtke, S.B. Pergher, J.H.Z. dos Santos, Zeolite NaA from Brazilian chrysotile and rice husk, Microporous Mesoporous Mater. 116 (2008) 548–554, https://doi.org/10.1016/j.micromeso.2008.05.014.

[31] J.J.F. Saceda, R.L. De Leon, K. Rintramee, S. Prayoonpokarach, J. Wittayakun, Properties of silica from rice husk and rice husk ash and their utilization for zeolite y synthesis, Quim. Nova 34 (2011) 1394–1397, https://doi.org/10.1590/S0100-40422011000800018.

[32] C. Zhang, S. Li, S. Bao, A facile and green method for the synthesis of hierarchical ZSM-5 zeolite aggregates from rice husk, Res. Chem. Intermed. 44 (2018) 3581–3595, https://doi.org/10.1007/s11164-018-3326-z.

[33] M.W. Anderson, S.M. Holmes, R. Mann, P. Foran, C.S. Cundy, Zeolitisation of diatoms, J. Nanosci. Nanotechnol. 5 (2005) 92–95, https://doi.org/10.1166/jnn.2005.022.

[34] M.A. Klunk, M. Das, S. Dasgupta, A.N. Impiombato, Comparative study using different external sources of aluminum on the zeolites synthesis from rice husk ash Comparative study using different external sources of aluminum on the zeolites synthesis from rice husk ash, Mater. Res. Express 7 (2020), 015023.

[35] M. Antonio, K. Suellen, B. Schröpfer, S. Dasgupta, M. Das, N. Roberto, A. Natale, I. Paulo, R. Wander, C. Alberto, M. Moraes, Synthesis and characterization of mordenite zeolite from metakaolin and rice husk ash as a source of aluminium and silicon, Chem. Pap. (2020), https://doi.org/10.1007/s11696-020-01095-4.

[36] S. Dai, L. Zhang, C. Hao, P. Qi, Preparation and characterization of zeolite/diatomite composite materials, Mater. Res. Express 6 (2019) 125516.

[37] S. Chotiwan, P. Somwongsa, S. Lao-ubol, P. Lao-auyporn, ScienceDirect Improvement of HZSM-5 catalytic performance by rice husk ash addition for methanol to hydrocarbons process, Mater. Today Proc. 17 (2019) 1354–1361, https://doi.org/10.1016/j.matpr.2019.06.155.

[38] D.H. Morawala, A.K. Dalai, K.C. Maheria, Synthesis of n - butyl levulinate using mesoporous zeolite H - BEA catalysts with different catalytic characteristics, Catal. Lett. 150 (2020) 1049–1060, https://doi.org/10.1007/s10562-019-03005-0.

[39] S.K. Jesudoss, J.J. Vijaya, P.I. Rajan, L.J. Kennedy, M. Mkandawire, Hierarchically pure and M (Cu, Ni) - impregnated ZSM-5 zeolites for the isomerization catalysis of n-hexane and 1-hexene, Mater. Res. Express 6 (2019) 125032.

[40] A.P. Pratama, D.U.C. Rahayu, Y.K. Krisnandi, Levulinic acid production from delignified rice husk waste over manganese Catalysts : Catalysts 10 (2020) 1–13.

[41] H. Ramezani, S.N. Azizi, G. Cravotto, Self-dual Leonard pairs Improved removal of methylene blue on modified hierarchical zeolite Achieved by a, Green Process. Synth. 8 (2019) 730–741.

[42] Y. Wang, H. Jia, P. Chen, X. Fang, T. Du, Synthesis of La and Ce modified X zeolite from rice husk ash for carbon dioxide capture, J. Mater. Res. Technol. 9 (2020) 4368–4378, https://doi.org/10.1016/j.jmrt.2020.02.061.

[43] S. Sivalingam, S. Sen, Sono-assisted adsorption of as (V) from water by rice-husk-ash- derived iron-modi fi ed mesoporous zeolite Y : a cradle-to-cradle solution to a problematic solid waste material, Ind. Eng. Chem. Res. 58 (2019) 14073–14087, https://doi.org/10.1021/acs.iecr.9b01785.

[44] H.F. Youssef, W.H. Hegazy, H.H. Abo-almaged, Preparation and characterization of micronized zeolite Na-A: cytotoxic activity of silver exchanged form, J. Porous Mater. 22 (2015) 1033–1041, https://doi.org/10.1007/s10934-015-9977-x.

[45] R. Amorim, N. Vilaça, O. Martinho, R.M. Reis, M. Sardo, J. Rocha, A.M. Fonseca, F. Baltazar, I.C. Neves, Zeolite structures loading with an anticancer compound as drug delivery systems, J. Phys. Chem. C 116 (2012) 25642–25650, https://doi.org/10.1021/jp3093868.

[46] N.A. Ghazi, K. Amir Hussain, N.A.N. Nik Malek, S. Hamdan, The effects of zeolite X and Y on cancer cell lines, J. Sci. Technol. 4 (2012) 33–40.

[47] S.K. Jesudoss, J. Judith Vijaya, K. Kaviyarasu, P. Iyyappa Rajan, S. Narayanan, L. John Kennedy, In-vitro anti-cancer activity of organic template-free hierarchical M (Cu, Ni)-modified ZSM-5 zeolites synthesized using silica source waste material, J. Photochem. Photobiol. B Biol. 186 (2018) 178–188, https://doi.org/10.1016/j.jphotobiol.2018.07.009.

[48] Z. Chen, J. Zhang, B. Yu, G. Zheng, J. Zhao, M. Hong, Amino acid mediated mesopore formation in LTA zeolites, J. Mater. Chem. A. 4 (2016) 2305–2313, https://doi.org/10.1039/c5ta09860b.

[49] M.I. Patel, R. Tuckerman, Q. Dong, A pitfall of the 3-(4,5-dimethylthiazol-2-yl)-5 (3-carboxymethonyphenol)- 2-(4-sulfophenyl)-2H-tetrazolium (MTS) assay due to evaporation in wells on the edge of a 96 well plate, Biotechnol. Lett. 5 (2005) 805–808, https://doi.org/10.1007/s10529-005-5803-x.

[50] S. Brunauer, P.H. Emmett, E. Teller, Adsorption of gases in multimolecular layers, J. Am. Chem. Soc. 60 (1938) 309–319, https://doi.org/10.1021/ja01269a023.

[51] Iza-Sc. http://www.iza-structure.com/databases/ (n.d.).

[52] B. Concepción-Rosabal, G. Rodríguez-Fuentes, N. Bogdanchikova, P. Bosch, M. Avalos, V.H. Lara, Comparative study of natural and synthetic clinoptilolites containing silver in different states, Microporous Mesoporous Mater. 86 (2005) 249–255, https://doi.org/10.1016/j.micromeso.2005.07.027.

[53] E. Sayah, D. Brouri, P. Massiani, A comparative in situ TEM and UV-visible spectroscopic study of the thermal evolution of Ag species dispersed on Al_2O_3 and NaX zeolite supports, Catal. Today 218–219 (2013) 10–17, https://doi.org/10.1016/j.cattod.2013.06.003.

[54] S. Hu, G. Song, D. Xue, F. Li, Influence of alkalinity on the synthesis of hierarchical LTA zeolite by using bridged polysilsesquioxane, RSC Adv. 9 (2019) 2551–2558, https://doi.org/10.1039/c8ra08952c.

[55] S. Iqbal, M. Fakhar-e-Alam, F. Akbar, M. Shafiq, M. Atif, N. Amin, M. Ismail, A. Hanif, W.A. Farooq, Application of silver oxide nanoparticles for the treatment of cancer, J. Mol. Struct. 1189 (2019) 203–209, https://doi.org/10.1016/j.molstruc.2019.04.041.

[56] J. Paunovic, D. Vucevic, T. Radosavljevic, S. Mandić-Rajčević, I. Pantic, Iron-based nanoparticles and their potential toxicity: focus on oxidative stress and apoptosis, Chem. Biol. Interact. 316 (2020) 108935, https://doi.org/10.1016/j.cbi.2019.108935.

[57] H. Peng, M. Ding, J. Vaughan, The anion effect on zeolite linde type A to sodalite phase transformation, Ind. Eng. Chem. Res. 57 (2018) 10292–10302, https://doi.org/10.1021/acs.iecr.8b02026.

[58] J. Mushtaq, R. Thurairaja, R. Nair, Bladder cancer, Surg. (United Kingdom). 37 (2019) 529–537, https://doi.org/10.1016/j.mpsur.2019.07.003.

[59] J.J. Meeks, H. Al-Ahmadie, B.M. Faltas, J.A. Taylor, T.W. Flaig, D.J. DeGraff, E. Christensen, B.L. Woolbright, D.J. McConkey, L. Dyrskjøt, Genomic heterogeneity in bladder cancer: challenges and possible solutions to improve outcomes, Nat. Rev. Urol. 17 (2020) 259–270, https://doi.org/10.1038/s41585-020-0304-1.

[60] Y. Takeyama, M. Kato, S. Tamada, Y. Azuma, Y. Shimizu, T. Iguchi, T. Yamasaki, M. Gi, H. Wanibuchi, T. Nakatani, Myeloid-derived suppressor cells are essential partners for immune checkpoint inhibitors in the treatment of cisplatin-resistant bladder cancer, Canc. Lett. 479 (2020) 89–99, https://doi.org/10.1016/j.canlet.2020.03.013.

[61] S. Castiglioni, A. Cazzaniga, C. Perrotta, J.A.M. Maier, Silver nanoparticles-induced cytotoxicity requires ERK activation in human bladder carcinoma cells, Toxicol. Lett. 237 (2015) 237–243, https://doi.org/10.1016/j.toxlet.2015.06.1707.

[62] P. Tavolaro, S. Catalano, G. Martino, A. Tavolaro, Zeolite inorganic scaffolds for novel biomedical application: effect of physicochemical characteristic of zeolite membranes on cell adhesion and viability, Appl. Surf. Sci. 380 (2016) 135–140, https://doi.org/10.1016/j.apsusc.2016.01.279.

[63] P. Tavolaro, G. Martino, S. Andò, A. Tavolaro, Zeolite scaffolds for cultures of human breast cancer cells. Part II: effect of pure and hybrid zeolite membranes on neoplastic and metastatic activity control, Mater. Sci. Eng. C 68 (2016) 474–481, https://doi.org/10.1016/j.msec.2016.06.013.

[64] C. Hepokur, İ.A. Kariper, S. Mısır, E. Ay, S. Tunoğlu, M.S. Ersez, Ü. Zeybek, S. E. Kuruca, İ. Yaylım, Silver nanoparticle/capecitabine for breast cancer cell treatment, Toxicol. Vitro 61 (2019), https://doi.org/10.1016/j.tiv.2019.104600.

[65] M.M. Saber, S.B. Mirtajani, K. Karimzadeh, Green synthesis of silver nanoparticles using Trapa natans extract and their anticancer activity against A431 human skin cancer cells, J. Drug Deliv. Sci. Technol. 47 (2018) 375–379, https://doi.org/10.1016/j.jddst.2018.08.004.

[66] P. Hernández, D. Alem, M. Nieves, H. Cerecetto, M. González, W. Martínez-López, M.L. Lavaggi, Chemosensitizer effect of cisplatin-treated bladder cancer cells by phenazine-5,10-dioxides, Environ. Toxicol. Pharmacol. 69 (2019) 9–15, https://doi.org/10.1016/j.etap.2019.03.015.

[67] S.K. Jesudoss, J.J. Vijaya, K. Kaviyarasu, L.J. Kennedy, R.J. Ramalingam, H.A. Al-lohedan, Anti-cancer activity of hierarchical ZSM-5 zeolites synthesized from rice-based waste materials, RSC Adv. 8 (2018) 481–490, https://doi.org/10.1039/c7ra11763a.

[68] L. Alban, W.F. Monteiro, F.M. Diz, G.M. Miranda, C.M. Scheid, E.R. Zotti, F. B. Morrone, R. Ligabue, New quercetin-coated titanate nanotubes and their radiosensitization effect on human bladder cancer, Mater. Sci. Eng. C 110 (2020) 110662, https://doi.org/10.1016/j.msec.2020.110662.

[69] Y.Y. Jia, J.J. Zhang, Y.X. Zhang, W. Wang, C. Li, S.Y. Zhou, B. Le Zhang, Construction of redox-responsive tumor targeted cisplatin nano-delivery system for effective cancer chemotherapy, Int. J. Pharm. 580 (2020) 119190, https://doi.org/10.1016/j.ijpharm.2020.119190.